Light-induced magnetic anisotropy in Co-doped garnet films

A. Stupakiewicz and A. Maziewski*
Institute of Experimental Physics, University of Bialystok, 41 Lipowa, 15-424 Bialystok, Poland

I. Davidenko
Interfaculty Research Laboratory of Information Recording Applied Problems, Kiev University, 60 Vladimirskaya, 252033 Kiev, Ukraine

V. Zablotskii†
Institute of Physics ASCR, Na Slovance 2, CZ-182 21 Praha 8, Czech Republic
(Received 16 January 2001; published 17 July 2001)

Light-induced uniaxial magnetic anisotropy characterized by amplitude, times of creation τ_1, and a vanishing τ_2 was studied. The investigation was performed on YIG (yttrium iron garnet):Co,Ca,Ge liquid-phase epitaxy films using a very sensitive method—observation of changes of magnetic domain structure with a different in-plane magnetization component induced by linearly polarized light pulses. An argon laser ($\lambda = 488$ nm) was used. The effective field H_L was introduced to describe the photoinduced uniaxial magnetic-anisotropy amplitude. These domain changes were studied within the temperature range of 160–300 K. With an increase in temperature an increase in τ_1, a decrease in τ_2, and a drastic decrease in H_L were found. The appearance of the photoinduced anisotropy is explained by light-induced rearrangement of strongly anisotropic Co^{2+} octahedral ions. A microscopic model was proposed where ion rearrangement is connected with electron excitations into the conducting band. Both thermal and light-induced excitations were discussed. Numerical and analytical solutions of kinetic equations describing the model are discussed. The dynamics of light-induced magnetic anisotropy both uniaxial and cubic is analyzed.

DOI: 10.1103/PhysRevB.64.064405 PACS number(s): 75.30.Gw, 75.60.Ch, 78.20.Ls

I. INTRODUCTION

Light-induced changes of magnetic ordering are important subjects for basic research and application. Most presented works have been connected with magnetic rearrangement by light-produced heating. However it seems that certain effects, when magnetic ordering could be changed by light without heating, are very interesting and important. Better understanding of these effects is one of the keys for magnetic-ordering ''engineering.'' In the present work we focus our attention on photomagnetic effects (PME's). At the same time, light-induced sample-temperature increase is not important. Photoexcited states and PME connected with them have been investigated in many systems, e.g., garnets, spinels, ferric borates, spin glasses, metal, magnetite, manganite, molecule-based magnets, etc.[1–7] Polarization-sensitive and -nonsensitive PME has been observed.[1] Primary attention has been given to photomagnetic study in magnetic garnets with tetravalent[1,8–10] (Si^{4+},Ge^{4+}) and divalent[11] (Ca^{2+}) dopants as well as in pure garnets.[10] Many years of study of garnets (polycrystals, bulks, and thin films) have resulted in a rather good understanding of their magnetic, optical, and electric properties. Therefore, garnets could be employed as model objects. Earlier PME investigations were limited to crystal garnets at cryogenic temperatures[1] ($T<150$ K). Only recently has polarization-sensitive photoinduced domain structure rearrangement at room temperatures in epitaxial films of Co-substituted yttrium iron garnets (YIG:Co) been discovered.[8] The influence of light on magnetic ordering is mainly performed by photoinduced changes of magnetic anisotropy. This can be observed in a system where anisotropy is connected with ions whose valence state could be changed by light. YIG:Co samples are good examples of such a system because Co^{2+} and Co^{3+} ions contribute to magnetic anisotropy differently. One can expect that light-induced electron redistribution between these ions changes the magnetic anisotropy of the sample. We showed in previous experiments[8] photoinduced electron redistribution between cobalt ions in octahedral nonequivalent states. It is easy to expect changes of cubic anisotropy by nonpolarized light due to a change in the general number of Co^{2+} (single cobalt Co^{2+} and Co^{3+} give huge and zero contribution to anisotropy, respectively). Polarized light can produce the appearance of uniaxial anisotropy in addition to possible changes in the cubic anisotropy. A systematic, experimental, and theoretical study of the dynamics of light-induced magnetic-anisotropy change is the aim of the present work. Magnetic-anisotropy creation and vanishing could be generally described by the characteristic times τ_1 and τ_2, respectively. Complex analysis of τ_1 and τ_2 is absent at the present time, especially as a temperature function. Such analysis is difficult using a traditional technique, for example, ferromagnetic resonance or torque anisometry because of their low sensitivity. The recently proposed magnetic-domain reconstruction analysis[8] under the influence of polarized light seems to be the best method for this purpose. In the present work, the investigations were extended for temperature and dynamics study using light pulses. The paper's organization is as follows. A sample characteristic and experimental setup is given in Sec. II where magnetic domain phases and their light-induced reconstruction are also discussed. Section III shows (i) the method of light-induced magnetic-anisotropy study by a light-pulses technique and (ii) experimental results. A micro-

scopic model describing photoinduced and thermal magnetic-ion redistribution is proposed in Sec. IV. Results achieved using the microscopic model are discussed in Sec. V.

II. SAMPLE AND EXPERIMENTAL SETUP

Experimental investigations were performed on film composed of $Y_2CaFe_{3.9}Co_{0.1}GeO_{12}$ with a thickness of 10 μm. These samples were grown by liquid-phase epitaxy on a paramagnetic substrate $Gd_3Ga_5O_{12}$ in plane (001). In the investigated film, doping with Ge^{4+} and Ca^{2+} ions was aimed at lowering the saturation magnetization and charge compensation, respectively.[12] These ions are localized in tetrahedral and dodecahedral sublattices accordingly. Cobalt and iron ions occupy octahedral and tetrahedral crystallographic positions. Cobalt could be in charged states Co^{2+}, Co^{3+}, and Co^{4+}, from which octahedral Co^{2+} is the most anisotropic[13] and Co^{4+} is rather rare.[14] The magnetic and optical properties of the investigated samples have been well-systematically characterized in many previous works[15–19,21–23] performed on these or similar samples. The vibrating sample magnetometer[15] study gave at room temperature saturation magnetization $4\pi M_S = 90$ Gs and the Neel temperature $T_N = 445$ K. Magnetic anisotropy has been investigated by ferromagnetic resonance spectroscopy,[16] torque magnetometry,[17] and magneto-optical magnetometry. The constants of cubic and uniaxial anisotropy at room temperature are, respectively, $K_1 = -10^4$ erg/cm^3, $K_U = -2.5 \times 10^3$ erg/cm^3. So, four easy magnetization-axis orientations slightly inclined from a $\langle 111 \rangle$ type of crystallographic direction to the sample plane exist. Temperature-induced reorientations of an easy magnetization axis were observed in the films.[17] The easy axis was oriented in-plane along a $\langle 110 \rangle$-type crystallographic direction below about 150 K. Results reported in the present paper were obtained within the temperature range 160–300 K. The optical and the Faraday-rotation spectra shows[18,19] that cobalt ions exist at different valency states (Co^{2+},Co^{3+}) and in crystallographic positions (octahedral and tetrahedral). Spectroscopy techniques determined the introduction of Co^{2+} and Co^{3+} ions in octahedral and tetrahedral positions.[18] Different types of magnetic domains corresponding to the directions of an easy magnetization axis were found in the investigated films. The existence of four domain phases P_A, P_B, P_C, and P_D (shown in Fig. 1) was observed in our previous experiments.[19]

Magnetic-domain phases have different in-plane magnetization components. Each magnetic phase is produced by applying the appropriate in-plane magnetic field[19] along proper $\langle 110 \rangle$-type direction. Transitions between phases P_A and P_B as well as between P_C and P_D take place during the change of magnetic-field direction into the opposite direction. The in-plane field induced a transition between P_A and P_B resulting in a shift of these phases boundaries, see Fig. 2. It is remarkable that similar shifts of phases boundaries can be realized by linearly polarized light (Fig. 3). In this case P_A/P_B, the magnetic phase is preferred to P_C/P_D.

The interphase boundary shift is explained by the appear-

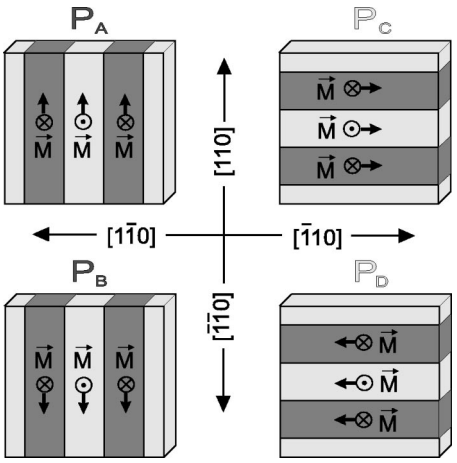

FIG. 1. Scheme of domain phases existing in YIG:Co film.

ance of the energy of light-induced magnetic anisotropy W_L under the influence of linearly polarized light,[8]

$$W_L = F_L(m_x m_y e_x e_y + m_x m_z e_x e_z + m_y m_z e_y e_z) + G_L(m_x^2 e_x^2 + m_y^2 e_y^2 + m_z^2 e_z^2) \quad (1)$$

where F_L and G_L are constants characterizing the light-induced anisotropy, and where e_i and m_i are the normalized components of light-polarization and magnetization vectors, respectively. According to Ref. 8, the effective field H_L applied along direction [110] is defined as

$$H_L = -F_L/(2M)\sin\theta\cos 2\varphi, \quad (2)$$

where θ and φ denote angles between (i) the magnetization M and [001] direction and (ii) the light-polarization plane and [100] direction, respectively.

The experimental setup was based on standard-polarization microscope elements. The sample was mounted in a closed-cycle cryostat ST-15 Cryomech with an antivi-

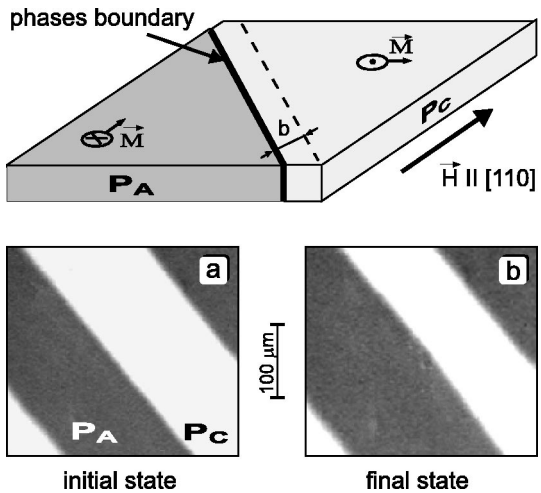

FIG. 2. Scheme and domain structure images before (a) and after (b) applying of in-plane field along [110] direction. In the photos, contrast between P_A and P_C phases is connected with a sample slightly inclined from the normal direction [001].

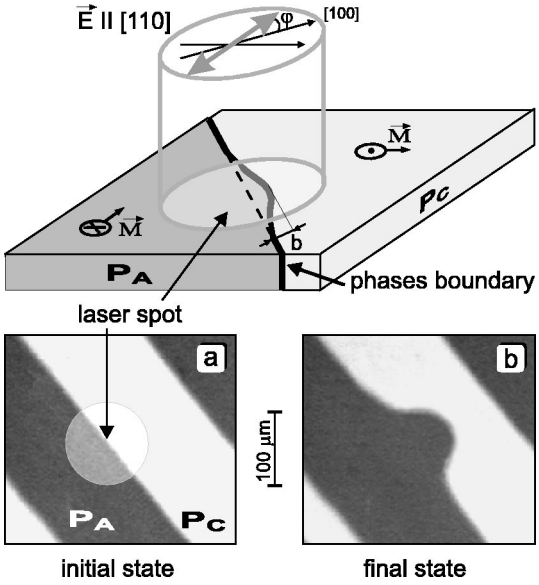

FIG. 3. Scheme and domain structure images before (a) and after (b) film illumination. In the photos contrast between P_A and P_C phases is connected with a sample slightly inclined from the normal direction [001].

brating system specially constructed for magneto-optical investigation. Within the investigated temperature range, the domain structure (DS) was observed by means of the Faraday effect. DS was visualized using a low-power halogen lamp, which does not produce any photoinduced DS changes. DS images obtained from a Mintron MTV-1801 charge-coupled device (CCD) camera were converted into digital format, 512×512 pixels, 256 gray levels using a Data Translation DT-3851 frame grabber. DS images were digitally processed specially to increase domain contrast.[20] The domain-pattern geometric parameters (stripe domain width, a domain area, parameters describing light-induced distortion of a domain wall, etc.) were digitally processed.

For PME excitation the sample was illuminated with an argon laser beam ($\lambda=488$ nm, light spot radius $R=50$ μm) focused on the film surface in the spatial region containing a boundary between domain phases. Figure 3 shows the scheme and DS images obtained from a CCD camera. Experiments were performed in both the stationary and pulse regimes. The laser light was switched mechanically or using a Pockels cell-based optical modulator. The system can produce (i) a sequence of pulses with light-pulse durations $t_1>0.03$ ms, dark-interval durations $t_2>0.3$ ms, and frequency of recurrence <1 kHz; and (ii) single pulses with adjustable duration $t_1>0.01$ ms. The laser beam (even without the halogen lamp) allows for investigation of dynamics of DS local changes corresponding to magnetization changes within the illuminated region. The pulse technique was developed to determine the time scale of light-induced magnetic-anisotropy growth and decay.

III. EXPERIMENTAL RESULTS

Experimental study of light-induced magnetic anisotropy is the main purpose of this section. The boundary between

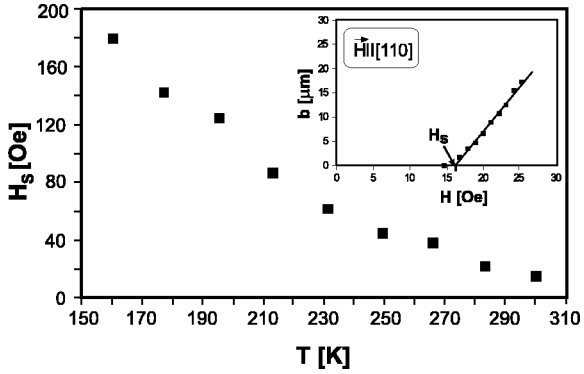

FIG. 4. Temperature dependence of the domain-wall-motion start field H_S. Inset shows determination of the start field H_S ($T=300$ K) by the extrapolation of the field dependence of the domain-wall-bend amplitude, $b(H)$.

P_A/P_B and P_C/P_D magnetic phases was used as a fine indicator sensitive to light response on a magnetic subsystem. We considered the state consisting of P_A and P_C phases. The interphase boundary was shifted by applying (i) an external in-plane magnetic field H along $[\bar{1}10]$ or $[110]$ directions and (ii) the effective field H_L produced by linearly polarized light (Fig. 3). The H_L field depends on the time of illumination. In the simplest way, H_L field creation could be described by the exponential law $H_L=H_L^{max}[1-\exp(-t/\tau_1)]$ after switching on the light at time $t=0$. The H_L field vanishes with another characteristic time as $\exp[-(t-t_1)/\tau_2]$ after switching off the light at $t=t_1$. General description of the temporal characteristics of photoinduced bending of the interface is rather complicated because, besides light-induced anisotropy, one should additionally take the domain-wall (DW) elasticity, coercivity, and magnetic after effects,[19,21] etc. into consideration. Therefore present investigations were focused on detecting the bending initiation by both the light and magnetic fields and the comparison of H_L and H. Photoinduced anisotropy was investigated in both quasistatic and light-pulse experimental regimes.

A. Quasistatic study

The boundary between the P_A and P_C phases moves upon the application of the field $H_{[110]}$ with an amplitude larger than the H_S—"starting-field"—value. The H_S growth with decrease in temperature is shown in Fig. 4.

The photoinduced shift of the boundary between the P_A and P_C phases has been investigated using linearly polarized light with a polarization direction along $[110]$ ($\varphi=45°$). The boundary between P_A and P_C phases moves when the light power P becomes higher than the P_S—"starting power"—value. The measured temperature dependence of P_S is shown in Fig. 5.

The amplitude of effective field H_L depends on the light power. The relation $H_L(P_S)=H_S$ is easily deduced. The $H_L(P)$ function was determined from the start of the shift of boundary between the P_A and P_C phases under the influence of both in-plane field $H_{[110]}$ and light $H_L(P)$ [$H_L(P)=H_S$

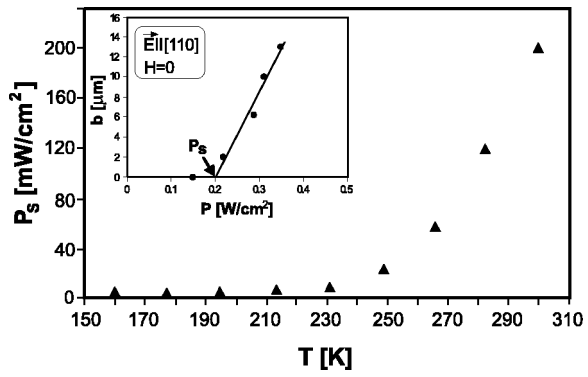

FIG. 5. Temperature dependence of light power P_S when the domain-wall-starts bending. Inset shows determination of start light power P_S ($T=300$ K) by the extrapolation of the light-power dependence of the domain-wall-bend amplitude $b(P)$.

$-H_{[110]}$]. The H_L^{max} amplitude is connected with the starting field H_S of domain bending, and light power P_S by the relation

$$H_L^{max}(T,P)=PH_S(T)/P_S(T). \tag{3}$$

Using Eq. (3) the temperature dependence of H_L^{max} was calculated for light power 0.2 W/cm^2. This value corresponds to P_S(300 K) (see Fig. 6).

B. Light-pulse regime study

Determination of τ_1 and τ_2 times characterizing the dynamic of light-induced anisotropy is the purpose of the study. Single-pulse experiments were performed for τ_1 reckoning. The interface boundary was illuminated by a light beam. Without an external magnetic field, a pulse power P larger than P_S was used to move the wall. The interface boundary started this bending when the light-pulse-duration was larger than t_{1S}. Exemplary domain wall shift measured as pulse duration function at $T=160$ K is shown in Fig. 7.

Magnetic-phase changes were also investigated applying both light pulses and the magnetic field. This was especially important for a low-light-power H_L study. The τ_1 was calculated using the relation

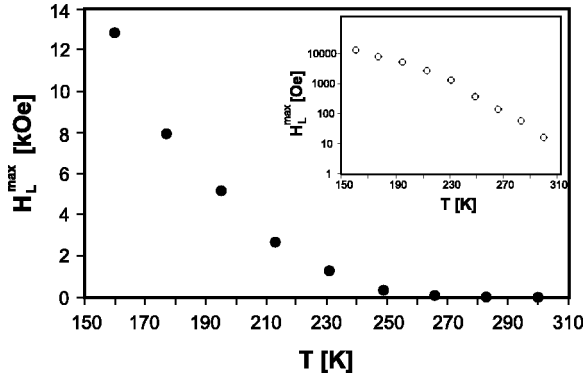

FIG. 6. Temperature dependence of the effective-field $H_L(T)$ amplitude determined for the power 0.2 W/cm^2. Inset shows the $H_L(T)$ dependence in a logarithmic scale.

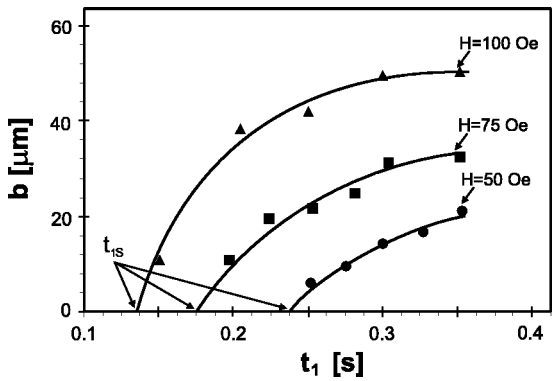

FIG. 7. Dependencies of DW shift amplitude on the single-light-pulse t_1 duration. $P=5$ mW/cm^2, $T=160$ K. The shift was registered for different amplitudes of external magnetic field $H_{[110]}$.

$$H_S=H+H_L^{max}(P)[1-\exp(t_{1S}/\tau_1)]. \tag{4}$$

Experiments allowed us to determine the dependencies of τ_1 on temperature and light power. Rise in τ_1 upon increase in temperature (see Fig. 8). A linear increase of $1/\tau_1$ under the growth of light-power amplitude was found (see Fig. 9).

Experiments with many light pulses were carried out to determine the time τ_2 characterizing vanishing of photoinduced anisotropy. A series of light pulses (with pulse duration t_1 and darkness interval t_2) induces changes of magnetic anisotropy[24] $H_L(t)$. A scheme of temporal $H_L(t)$ changes induced by light pulses is shown in Fig. 10. After many light pulses, the H_L amplitude increases tending to the following H_{L2} value:

$$H_{L2}(t_1,t_2)=\frac{1-\exp(-t_1/\tau_1)}{1-\exp(-t_1/\tau_1)\exp(-t_2/\tau_2)}H_L^{max}. \tag{5}$$

Similarly to the previous description, the beginning of photoinduced bending of the interface boundary was found after many light pulses. The temperature dependence of time τ_2 determined from experiments is shown in Fig. 11. τ_2 decreases under temperature growth.

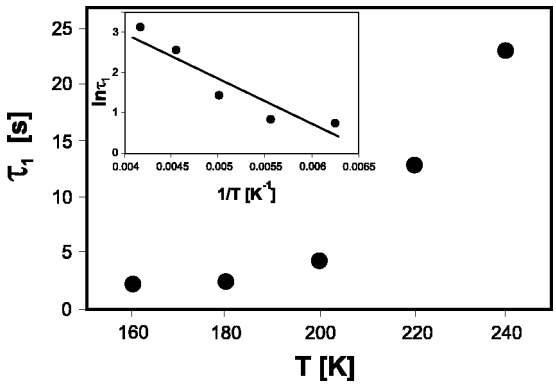

FIG. 8. Temperature dependence of the light-induced anisotropy creation time τ_1. Inset shows $\ln(\tau_1)$ as a function of $1/T$.

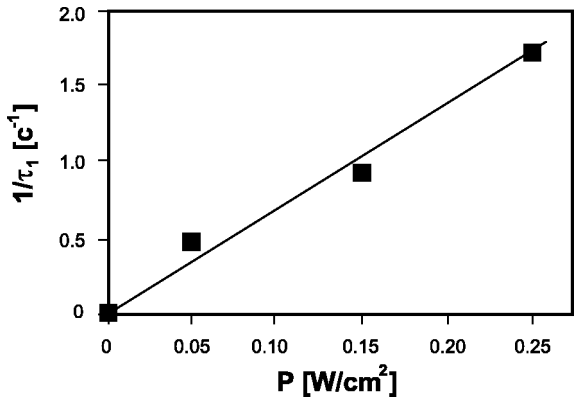

FIG. 9. Dependence of $1/\tau_1$ on the light power amplitude.

IV. MICROSCOPIC MODEL

The model described below is valid for the general case of a semiconductor or an isolator doped by ions "*I*" located in two orientationally inequivalent *X* and *Y* sites of a crystal lattice. The basic assumptions of the model are the following: (i) a mixture of ions could exist in a different valence state $I^{(m+1)+}$ and I^{m+} giving different contributions to magnetic anisotropy; (ii) linearly polarized light excites these ions with a probability, which is generally different for the *X* and *Y* positions. Other defected samples (e.g., vacancies with properties similar to those described above) could also be considered in the model instead of dopant ions. The example of cobalt ions (in Co^{2+} and Co^{3+} states) occupying garnet octahedral sides will be considered later on in the paper. Schematic presentation of the possible electron transitions in the considered system with their respective probabilities is shown in Fig. 12. ω_{0x} and ω_{0y} are the probabilities of the light-induced electron transitions from Co^{2+} ions placed, respectively, in *X* and *Y* positions into the conductive band *Z*. ω_2 is the probability of an electron excitation toward the band by a thermally activated process. ω_{1x} and ω_{1y} are the probabilities of opposite transitions from band *Z* into positions *X* and *Y*, respectively.

A redistribution of total *N* dopant ions is described by the system of kinetic equations,

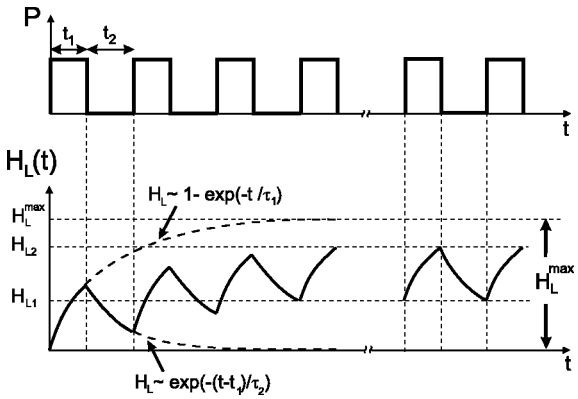

FIG. 10. Changes in effective field H_L induced by light pulses.

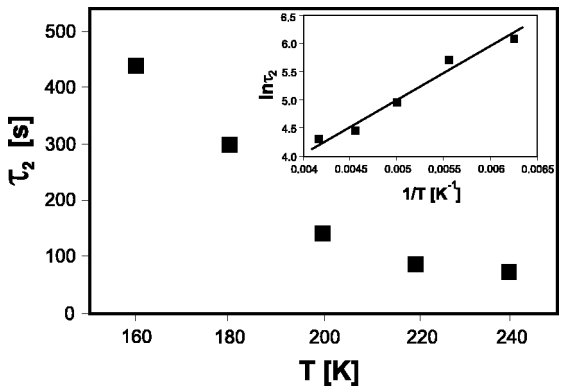

FIG. 11. Temperature dependence of the light-induced-anisotropy vanishing time τ_2. Inset shows $\ln(\tau_2)$ as a function of $1/T$.

$$\frac{dn_{2x}}{dt} = -\omega_{0x}n_{2x} + \omega_{1x}n_z - \omega_2 n_{2x},$$

$$\frac{dn_{2y}}{dt} = -\omega_{0y}n_{2y} + \omega_{1y}n_z - \omega_2 n_{2y}, \tag{6}$$

$$\frac{dn_z}{dt} = (\omega_2 + \omega_{0x})n_{2x} + (\omega_2 + \omega_{0y})n_{2y} - (\omega_{1x} + \omega_{1y})n_z,$$

where the concentrations (normalized to $0.5N$) (i) n_{2x} and n_{2y}—Co^{2+} ions in the *X* and *Y* positions, respectively; (ii) n_{3x} and n_{3y}—Co^{3+} ions in the *X* and *Y* positions, respectively; and (iii) n_z—electrons in the conductive band were taken into account. It should be pointed out that the system of kinetic equations like Eqs. (6) is commonly used for electron transitions in a three-level microscopic system for description of photoinduced changes of occupancies of states

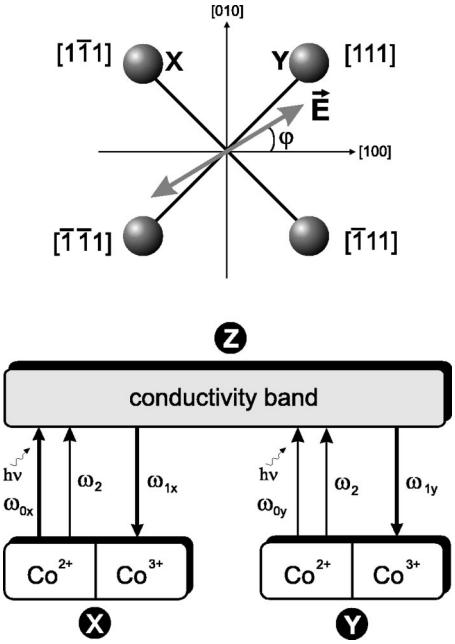

FIG. 12. Schematic illustration of excitation of Co^{2+} ions in octahedral *X* and *Y* positions. Electric vector $\vec{E}$ of linearly polarized light is marked.

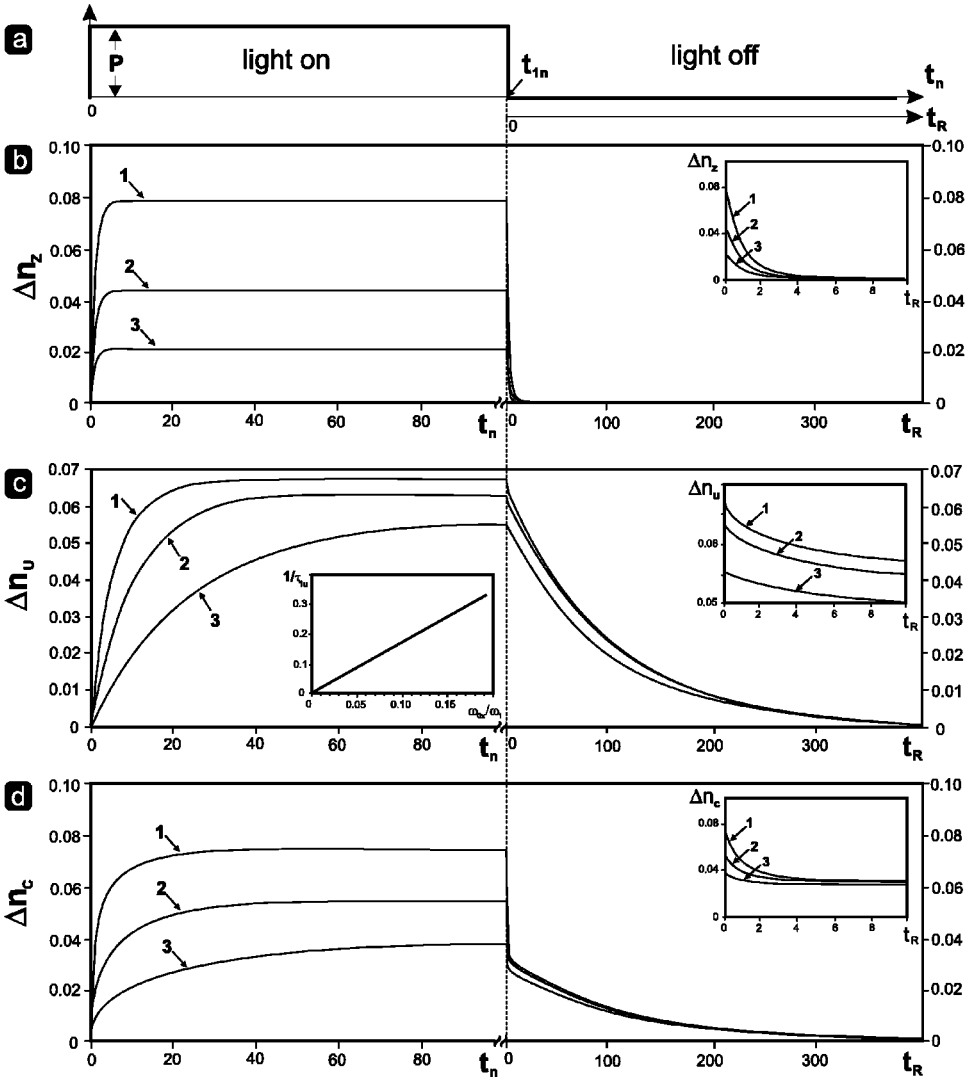

FIG. 13. Illustration of charge redistribution induced by linearly polarized light ($\varphi=45°$): (a) light pulse; time dependence of the following concentration changes, (b) $\Delta n_z(t_n)$ electrons in conducting band; parameters responsible for light induced (c) $\Delta n_u(t_n)=n_{2y}(t_n)-n_{2x}(t_n)$—uniaxial anisotropy (the inset shows dependence of $1/\tau_1$ on the light power amplitude P); and (d) $\Delta n_c(t_n)=n_{2x}(0)-n_{2x}(t_n)$—cubic anisotropy. Curves were calculated for normalized ($\omega_1=1$) $\omega_2=0.005$ and different values of ω_{0x} (proportional to light power P) as follows: (1) $\omega_{0x}=0.1$, (2) $\omega_{0x}=0.05$, (3) $\omega_{0x}=0.02$.

with different energies resulting in changes of photoconductivity, absorption, birefringence, etc. The conservation of the total charge gives the relation

$$n_{2x}(t)+n_{2y}(t)+n_z(t)=n_2, \tag{7}$$

where n_2 is the total Co^{2+} concentration without light at $T=0$ K. The discussed probabilities could be written in the following form:

$$\omega_{0x}=\Gamma P[1+B(1-\sin 2\varphi)/2], \tag{8a}$$

$$\omega_{0y}=\Gamma P[1+B(1+\sin 2\varphi)/2], \tag{8b}$$

$$\omega_{1x}=\omega_1\beta n_{3x}, \quad \omega_{1y}=\omega_1\beta n_{3y}, \tag{8c}$$

where φ is the angle between the light polarization direction $\vec{E}$ and dipole momentum of ions in the X and Y sites, P is the light intensity, B is the phenomenological constant, β is the frequency parameter, and Γ is a numerical coefficient. A similar description was used in [25]. Equal concentrations of anisotropic ions in both the X and Y positions before illumination ($t\leqslant 0$) is assumed; $n_{2x}(0)+n_{3x}(0)=n_{2y}(0)+n_{3y}(0)=1$.

Without illumination, electrons are transferred into the Z band only by the thermal activation process. Because $\omega_2/\omega_1\ll 1$ this electron concentration is small and equal $n_z(0)=\omega_2 n_{2x}/(\omega_1 n_{3x})$. Let us discuss the linearly polarized light-pulse-induced changes of the microscopic system. The light, linearly polarized along $\varphi=45°$, switched on at $t=0$ prefers Co^{2+} ions excitations in the X position rather than in the Y position, see Fig. 12. The light-induced changes of the microscopic system will in the first step be illustrated by numerical simulations. These simulations were performed for both illumination power, Fig. 13, and temperature Fig. 14. Some analytical Eq. (6) solutions will also be shown in the second step of our discussion.

After the light is switched on, the electrons are excited from X,Y positions—n_z changes concentration, see Figs. 13(b) and 14(b). The dynamics of concentration changes have been approximated by exponential functions to compare different τ. Figures have been drawn using the normalized time ($t_n=t\omega_1$). A different efficiency of polarized-light-induced excitation of ions placed in X,Y positions gives $\Delta n_u(t)=n_{2y}(t)-n_{2x}(t)$. The Δn_u parameter describes the light-induced uniaxial anisotropy studied in our experiments.

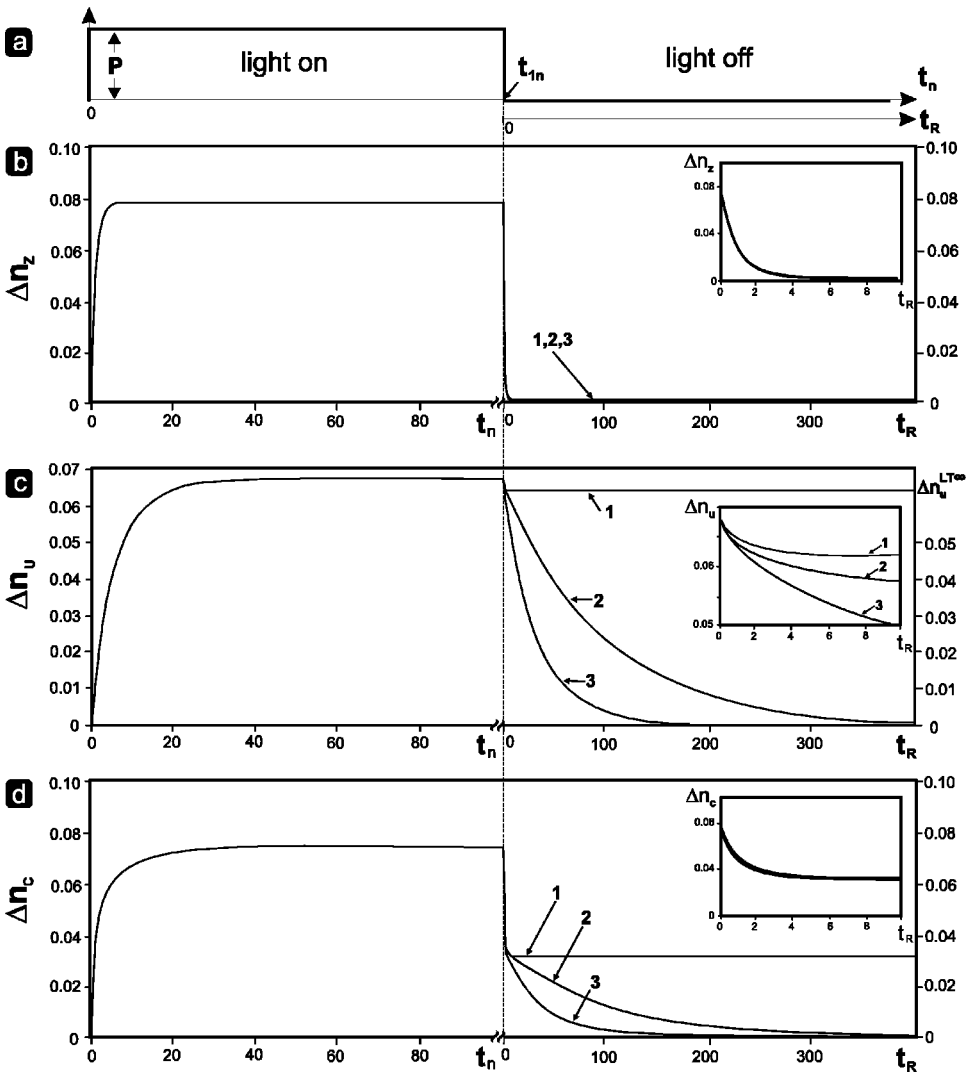

FIG. 14. Illustration of charge redistribution induced by linearly polarized light ($\varphi=45°$): (a) light pulse; time dependence of the following concentration changes, (b) $\Delta n_z(t_n)$ electrons in conducting band; parameters responsible for light induced (c) $\Delta n_u(t_n)=n_{2y}(t_n)-n_{2x}(t_n)$—uniaxial anisotropy; and (d) $\Delta n_c(t_n)=n_{2x}(0)-n_{2x}(t_n)$—cubic anisotropy. Curves were calculated for normalized ($\omega_1=1$) $\omega_{0x}=0.01$ and different values of ω_2 (related to different temperatures) as follows: (1) $\omega_2=0$ ($T=0K$), (2) $\omega_2=0.008$, (3) $\omega_2=0.015$.

The $\Delta n_u(t)$ is approximated by $\Delta n_u^{max}[1-\exp(-t/\tau_{1u})]$, see Fig. 13(c). The velocity of the photoinduced uniaxial anisotropy creation (described by the value $1/\tau_{1u}$) increases with light power. For increasing light power P, the $1/\tau_{1u}$ parameter increases linearly, see inset in Fig. 13(c). One can expect this from the assumption in Eq. (8a). The light-induced cubic-anisotropy changes are connected with the parameter $\Delta n_c(t)=n_{2x}(0)-n_{2x}(t)$. For condition $n_{2x}(0)=n_{2y}(0)$, $\Delta n_c(t)=[\Delta n_z(t)+\Delta n_u(t)]/2$. Figures 13(d) and 14(d) show the temporal dependence of the concentration Δn_c.

Let us now consider our system after the light is switched off at $t_n=t_{1n}$ ($t_R=t_n-t_{1n}$ is now used), see Fig. 13(a). Fast electron return from the conducting band is observed in Figs. 13(b) and 14(b). Two steps of light-induced uniaxial anisotropy vanishing could be distinguished: (i) fast vanishing that could be characterized by τ_{2u}^{fast} time in exponential approximation, see the inset in Figs. 13(c) and 14(c), and (ii) slow vanishing described by the τ_{2u}^{slow} time. Changes of the Δn_c concentration also happen in two similar steps. The general analytical description of the microscopic system given by Eqs. (6) is complicated. Analytical solutions will be discussed below for relaxation of a light-excited system when the light is switched off. Taking into account that $\omega_{0x}=\omega_{0y}=0$ one can find the solution of Eqs. (6) in the form

$$\Delta n_u(t_R)=\frac{k\exp\left(\frac{t_R}{\tau_2'}\right)\operatorname{sech}\left(\frac{t_R}{\tau_2''}-\operatorname{arctanh}\left\{\frac{\tau_2''}{2}[(2c-3)\omega_1-\omega_2]\right\}\right)}{\tau_2''\sqrt{\omega_1[c\omega_2-\omega_1(2-c)(c-1)]}}, \tag{9a}$$

$$n_z(t_R)=-\frac{1}{2}-\frac{\omega_2}{2\omega_1}+\frac{1}{\tau_2''\omega_1}\tanh\left(\frac{t_R}{\tau_2''}+\operatorname{arctanh}\left\{\frac{\tau_2''}{2}[3\omega_1+\omega_2-2c\omega_1]\right\}\right), \tag{9b}$$

where

$$\tau_2' = \frac{2}{\omega_1 - \omega_2}, \quad \tau_2'' = \frac{2}{\sqrt{(\omega_1+\omega_2)^2 + 4\omega_1\omega_2}}, \tag{10}$$

$c = n_{2y}(t_R=0) + n_{2x}(t_R=0), k = \Delta n_u(t_R=0)$, and time t_R is calculated from the moment of the light switching off. It is easily seen from Eq. (9a) that two characteristic times τ_2' and τ_2'' determine the relaxation of $\Delta n_u(t_R)$. Let us consider this relaxation in small and large time scales expending Eq. (8a) for $t_R \ll \tau_2', \tau_2''$ and $t_R \gg \tau_2', \tau_2''$, respectively. Only the time τ_2' determines fast Δn_u relaxation ($\tau_{2u}^{fast} = \tau_2'$). The Δn_u relaxation after a long time is defined by the characteristic time τ_{2u}^{slow} dependent on both τ_2' and τ_2'' as follows:

$$\tau_{2u}^{slow} = \frac{\tau_2'\tau_2''}{\tau_2' - \tau_2''}. \tag{11}$$

Evidently, we can deduce that $\tau_2' \geqslant \tau_2''$ and τ_{2u}^{slow} is much larger than τ_2'. The difference between τ_{2u}^{fast} and τ_{2u}^{slow} strongly depends on temperature Fig. 14(c). It follows from Eqs. (10) that $\tau_2' = \tau_2''$ in the low-temperature limit ($\omega_2 \to 0$). This means that $\tau_{2u}^{slow} \to \infty$ and part of the light-induced uniaxial anisotropy (remaining after the first-step fast relaxation) practically never relaxes to zero [see Figs. 14(c) and 14(d), curves 1]. $1/\tau_{2u}^{slow}$ could be approximated by $2\omega_2$ for a lower temperature. From Eq. (9a) one can obtain $\Delta n_u^{LT\infty}$, the difference between concentrations of Co^{2+} in the Y and X positions at $T=0$ and $t_R \to \infty$ in the following form: $\Delta n_u^{LT\infty} = \Delta n_u(t_R=0)/[2 - n_2 + n_z(t_R=0)]$. The value $\Delta n_u^{LT\infty}$ determines the ''frozen'' part of light-induced uniaxial anisotropy. This part is connected with $\Delta n_u(t_R=0)$ as well as with the concentration of electrons in the conducting band at $t_R=0$. The case of temporal, stable, low-temperature, light-induced anisotropy is similar to the case of room-temperature, temporal-stable, growth-induced anisotropy obtained for different magnetic systems.[34]

V. DISCUSSION AND CONCLUSION

In contrast to earlier investigated garnets[1,9–11] with tetravalent dopants (YIG:Si), divalent dopants (YIG:Ca), and pure YIG, photomagnetism in YIG:Co has been observed in a much wider temperature range: from liquid helium to room temperature.[8,26] It is evident that the distinction of the temperature ranges of PME existence in such materials is a consequence of the different nature of light-sensitive anisotropic-impurity centers responsible for PME. This allows the supposition, that the existence of high-temperature polarization-dependent PME in YIG:Co is determined only by the presence of cobalt ions in the garnet matrix.

The symmetry of PME dependency on light polarization[8] indicates that light-sensitive anisotropic centers occupy the octahedral sites in the crystal lattice because its minima correspond to polarization directions where the probability of photoexcitation of octahedral centers is the largest. It is known[14,27] that Co^{2+}, Co^{3+}, and Fe^{3+} ions can be found in these positions. An octahedral Co^{3+} ion gives a zero contribution to the total magnetic anisotropy in a single-ion approximation. The contribution of octahedral Co^{2+} results in three ranges of magnitude larger than with Fe^{3+}.[13,14] Thus, it would be natural to suppose that photoinduced anisotropy appearance and respective magnetization changes are connected with Co^{2+}-ion redistribution amongst the octahedral sites of the garnet lattice. Ion Co^{2+} has a stable valency in the garnet matrix because its energetic $3d$ levels do not coincide with $3d$ levels of iron ions and weakly resonate with them. The energy level of the octahedral ion Co^{2+} is situated ~ 1 eV below the edge of the conductivity band.[28] This makes electron transitions between cobalt ions difficult. Under the influence of light these transitions can be accomplished through the conductivity band.

Let us discuss the experimentally determined temperature dependence of parameters describing photoinduced anisotropy: amplitude, creation time τ_1, and vanishing time τ_2. At increasing temperatures, τ_2 decreases, see Fig. 11. In our model τ_2 corresponds to τ_{2u}^{slow}, which is approximated by $1/(2\omega_2)$. The description of thermal electron excitation probability is usually assumed[29,30] as follows: $\omega_2 = \nu \exp(-E_{A2}/kT)$, where E_{A2} is the activation energy of thermoactivated electron transition and ν is the frequency factor. The exponential curve $\tau_2 = C_2 \exp(E_{A2}/kT)$ fits these experimental data at $E_{A2} = 0.084 \pm 0.008$ eV, $C_2 = 1.4 \pm 0.2$ s. The E_{A2} energy is much smaller than 1 eV. So it is natural to expect that in our samples, different defects produce additional energy levels enabling easier electron relaxation. A similar explanation was proposed for PME description in $CdCr_2Se_4$.[4]

At larger light intensities P the photoinduced anisotropy appears faster. Linear dependence of $1/\tau_1$ on P was found both in experiment and theory, see Figs. 9 and 13. Similar results were also obtained in Ref. 1.

Temperature dependence of the velocity of the photoinduced anisotropy creation has not been studied up to now. At increasing temperatures, τ_1 increases, see Fig. 8. The uniaxial photoinduced anisotropy appearance is connected with electron transfer between cobalt ions at different sites.[31] At increasing temperatures, electron-phonon interaction prevents the transfer. At increasing temperatures, a decrease in charge-carrier mobility in semiconductors has been observed,[32] which was explained by an increase of electron scattering by phonons. The decrease in mobility was described by the exponential law $\exp(E_P/kT)$, where E_P is the phonon energy. A similar expression could be used for the description of photoinduced anisotropy changes: $1/\tau_1 = C_1 \exp(E_{A1}/kT)$. This dependence fits our points at $E_{A1} = 0.11 \pm 0.03$ eV, which is a typical value for optical phonons.[33]

At decreasing temperatures, a strong increase of amplitude of the effective photoinduced field H_L^{max} was observed, see Fig. 6. This effect could be explained by (i) increase of single-ion contribution to magnetic anisotropy[13,35] and (ii) more efficient light-induced charge redistribution in lower temperatures. The redistribution is less disturbed by interaction with phonons than was suggested above.

Our proposal for analysis of magnetic DS changes under the influence of linearly polarized light pulses is an extremely sensitive method for the photomagnetic-effect study. We conducted a complex study of temporal and temperature changes of photoinduced uniaxial magnetic anisotropy on epitaxial film YIG:Co. Characteristic phenomenological parameters describing the anisotropy were determined as a result.

The proposed microscopic model enables the description of light-induced changes of both uniaxial- and cubic-anisotropy terms. The changes take place on different time scales.

Our study shows that light-induced, local, reversible engineering of magnetic properties is possible. For example, using light pulses with a properly defined duration, polarization, and amplitude, one can locally create for different times a useful type of magnetic anisotropy and/or locally magnetize a sample. Testing these ideas on other materials could be interesting.

ACKNOWLEDGMENTS

The authors are indebted to Professor P. Görnert for providing samples. One of the authors (I.D.) was partially supported by Grant No. INTAS 97-0366.

*Electronic address: magnet@cksr.ac.bialystok.pl
†Also at Physics Department, Donetsk National University, St. Universitetskaya 24, 83055 Donetsk, Ukraine.

[1] V. F. Kovalenko and E. L. Nagaev, Usp. Fiz. Nauk. **148**, 561 (1986) [Sov. Phys. Usp. **29**, 297 (1986)]; E. L. Nagaev, Phys. Status Solidi B **145**, 11 (1988), and references therein.
[2] P. F. Bongers and U. Enz, Phys. Rev. Lett. **21**, 1643 (1968).
[3] M. Ayadi and J. Ferre, Phys. Rev. Lett. **50**, 274 (1983).
[4] E. Mosiniewicz-Szablewska and H. Szymczak, Phys. Rev. B **47**, 8700 (1993).
[5] M. Baran, S. L. Gnatchenko, A. R. Kaul, R. Szymczak, and H. Szymczak, Phys. Rev. B **60**, 9244 (1993).
[6] D. A. Pejakovic, J. L. Manson, J. S. Miller, and A. J. Epstein, Phys. Rev. Lett. **85**, 1994 (2000).
[7] H. Szymczak, M. Baran, S. L. Gnatchenko, R. Szymczak, Y. F. Chen, Z. G. Ivanov, and L-G. Johansson, Europhys. Lett. **35**, 451 (1996).
[8] A. B. Chizhik, I. I. Davidenko, A. Maziewski, and A. Stupakiewicz, Phys. Rev. B **57**, 14 366 (1998).
[9] K. Hisatake, I. Matsubara, K. Maeda, H. Yasuoka, T. Mazaki, T. Miyazaki, and S. Kainuma, J. Phys. IV **8**, 367 (1998).
[10] V. G. Veselago, R. A. Doroshenko, and S. G. Rudov, Zh. Eksp. Teor. Fiz. **105**, 638 (1994) [JETP **78**, 341 (1994)].
[11] M. Pardavi-Horvath, P. E. Wigen, and G. Vértesy, J. Appl. Phys. **63**, 3110 (1988).
[12] P. Görnert, M. Nevřiva, J. Šimšova, W. Andrä, W. Schüppel, P. Šumšal, and B. Bubákowá, Phys. Status Solidi A **74**, 107 (1982).
[13] *Numerical Data and Functional Relationships in Science and Technology*, edited by P. Hansen, K. Enke, and G. Winkler, Landolt-Bornstein, New Series, Group III, Vol. 12 (Springer-Verlag, Berlin, 1978).
[14] M. D. Sturge, E. M. Gyorgy, R. C. LeCraw, and J. P. Remeika, Phys. Rev. **180**, 413 (1969).
[15] A. Maziewski, L. Půst, and P. Görnert, J. Magn. Magn. Mater. **83**, 87 (1990).
[16] M. Marysko, P. Görnert, and J. Paces, Phys. Status Solidi A **123**, 303 (1991).
[17] M. Tekielak, W. Andrä, A. Maziewski, and J. Taubert, J. Phys. IV **7**, 461 (1997); J. Phys. III **C1**, C461 (1997).
[18] Z. Šimša, IEEE Trans. Magn. **MAG-23**, 3323 (1987).
[19] A. Maziewski, J. Magn. Magn. Mater. **88**, 325 (1990).
[20] A. Maziewski, K. Mroczek, A. Stankiewicz, M. Tekielak, and M. Kisielewski, Fiz. Nizk. Temp. **18**, Suppl. S1 (1992).
[21] M. Kisielewski, A. Maziewski, and P. Görnert, J. Phys. D **20**, 222 (1987).
[22] B. Ivanov, M. Kisielewski, S. Lyakhimets, and A. Maziewski, Zh. Eksp. Teor. Fiz. **101**, 1894 (1992) [Sov. Phys. JETP **74**, 1013 (1992)].
[23] A. Maziewski, in *Ferrites*, Proceedings of ICF'6, Tokyo, 1992, edited by T. Yamaguchi and M. Abe, p. 782.
[24] I. I. Davidenko, A. Maziewski, and A. Stupakiewicz, J. Magn. Magn. Mater. **196-197**, 828 (1999).
[25] M. Wurlitzer and J. Franke, Phys. Status Solidi A **64**, 539 (1981).
[26] F. K. Lotgering, Phys. Chem. Solids **36**, 1183 (1975).
[27] B. Antonini, M. Marinelli, E. Milani, A. Paoletti, P. Parolli, J. Daval, and B. Ferrand, Phys. Rev. B **39**, 13 442 (1989).
[28] G. H. Jonker, J. Phys. Chem. Solids **9**, 325 (1959).
[29] R. P. Hunt, J. Appl. Phys. **38**, 2826 (1967).
[30] V. F. Kovalenko, S. N. Lyakhimets, and P. S. Kuts, Fiz. Tverd. Tela (Leningrad) **24**, 2428 (1982) [Sov. Phys. Solid State **24**, 1379 (1982)].
[31] P. Hansen, W. Tolksdorf, and R. Krishnan, Phys. Rev. B **16**, 3973 (1977).
[32] L. Schein and A. McGhie, Phys. Rev. B **20**, 1631 (1979).
[33] V.S. Vavilov, N.P. Kekelidze, and L.S. Smirnov, *Dejstvie izluchenij na poluprovodniki* (Nauka, Moskva, 1988).
[34] A. Eschenfelder, *Magnetic Bubble Technology*, edited by H.-J. Queisser, Springer Series in Solid State Sciences, Vol. 14 (Springer, Berlin, 1981).
[35] J. C. Slonczewski, Phys. Rev. **110**, 1341 (1958).